

Engineering Second-Order Nonlinear Optical Activity by Means of a Noncentrosymmetric Distortion of the [Te–N]₂ Supramolecular Synthons

Anthony F. Cozzolino, Qin Yang, and Ignacio Vargas-Baca*

Department of Chemistry and Chemical Biology, McMaster University, 1280 Main Street West, Hamilton, Ontario L8S 4M1, Canada

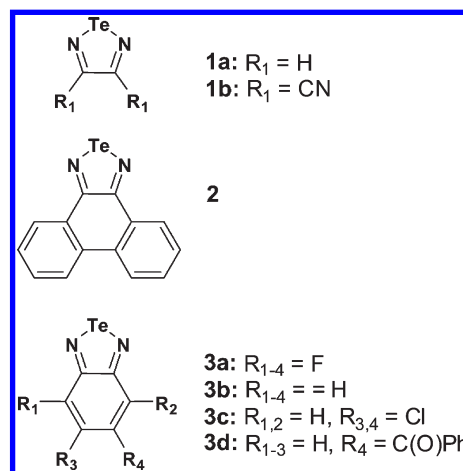
Received August 12, 2010; Revised Manuscript Received September 20, 2010

ABSTRACT: Moderate steric repulsion within the supramolecular ribbon chains assembled by 1,2,5-telluradiazole derivatives causes a distortion of the [Te–N]₂ supramolecular synthon which removes the inversion center from the four-membered virtual ring. This geometrical feature can propagate through the lattice, creating a noncentrosymmetric crystal with second-order nonlinear optical (NLO) properties. This principle was demonstrated in the cases of 3,4-dicyano-1,2,5-telluradiazole and 5,6-dichlorobenzo-2,1,3-telluradiazole. The second harmonic generation efficiency of these materials, however, is modest because the molecular dipole moments have a nearly antiparallel arrangement in the ribbons. The structure of 5-benzoylbenzo-2,1,3-telluradiazole demonstrates that it is indeed possible to extend this strategy to generate acentric crystals of benzo-2,1,3-telluradiazoles featuring pendant groups (including NLO chromophores) and in this way design more efficient NLO materials.

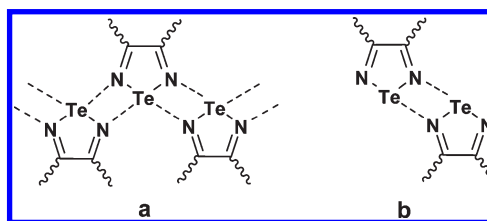
Introduction

In the crystal structures, 1,2,5-telluradiazole (**1a**, Chart 1) and its annulated derivatives exhibit intermolecular association, forming ribbon chains and, in sterically encumbered cases, dimers (Scheme 1).^{1–4} The supramolecular structural element that builds these arrangements—the *supramolecular synthon*⁵—is a virtual four-membered ring that features two antiparallel Te···N secondary bonding interactions (SBIs). The binding energy of the [Te–N]₂ supramolecular synthon is large enough to induce a geometric distortion of the aromatic system in phenanthro(9,10-*c*)-1,2,5-telluradiazole (**2**) in order to accommodate the formation of the ribbon.³ In a case with smaller but still significant steric repulsion, 4,5,6,7-tetrafluorobenzo-2,1,3-telluradiazole (**3a**) assembles ribbon chains which appear significantly distorted as compared to the ribbons in the structure of benzo-2,1,3-telluradiazole (**3b**).² Two types of distortion of the [Te–N]₂ supramolecular synthon lead to distinct crystalline polymorphs of **3a**. One phase (β) features centrosymmetric [Te–N]₂ supramolecular synthons with longer (2.8 Å) Te···N SBIs; this array is metastable and switches to the thermodynamically preferred structure by a thermochromic phase transition.⁶ In the α phase, all the [Te–N]₂ supramolecular synthons are equal but distorted and the ribbons are puckered. The overall distortion in this case is best described as the combination of two motions: one is an in-plane motion that produces two different SBI lengths (Scheme 2a), and the other is a rotation of the rings with respect to each other (Scheme 2b). Each of these distortions on its own implies the removal of the inversion center of the [Te–N]₂ supramolecular synthon. Even though the overall lattice of α -**3a** is racemic and thus centrosymmetric, if this feature were to propagate throughout the lattice by virtue of other intermolecular interactions and packing, the result would be a noncentrosymmetric crystal. Here we report that it is indeed possible to take advantage of such steric effects to promote crystallization in a

Chart 1



Scheme 1. Supramolecular Assemblies of 1,2,5-Telluradiazoles Formed by the [Te–N]₂ Supramolecular Synthons: (a) Ribbon Chain; (b) Dimer



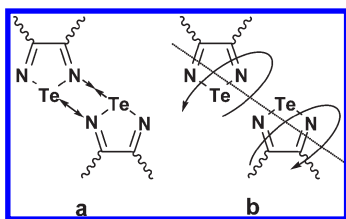
noncentrosymmetric lattice with the consequent second-order nonlinear optical activity.

Experimental Section

Materials and Methods. All starting materials were reagent grade and were used as received unless it is otherwise stated. Diaminomaleonitrile, 1,2-diamino-4,5-dichlorobenzene, 3,4-diaminobenzophenone, and pyridine were purchased from Aldrich. Triethylamine was purchased from Anachemia; toluene and methylene chloride

*Corresponding author. Telephone: 905 525 9140, ext 23497. Fax: 905 522 2509. E-mail: vargas@chemistry.mcmaster.ca.

Scheme 2. Non-centrosymmetric Distortions of the [Te–N]₂ Supramolecular Synthons: (a) In-Plane; (b) Out-of-Plane



were purchased from Caledon. TeCl₄ was prepared by reaction of Cl₂ with elemental Te purchased from Cerac. Pyridine and triethylamine were dehydrated over CaH₂ before use, and the toluene and methylene chloride were passed through an Innovative Technologies solvent purification system. The manipulation of air sensitive materials was performed under an atmosphere of anhydrous argon or nitrogen with standard Schlenk and glovebox techniques.

General Instrumentation. IR spectra were recorded on a Nicolet 6700 FT-IR spectrometer with a resolution of 4 cm⁻¹. Raman spectra were acquired with a Renishaw Invia spectrometer exciting at 785 nm, 30 mW, averaging 10 scans (10 s each). The ¹H and ¹³C NMR spectra were acquired on a Bruker AV200 (200.13 MHz) spectrometer or a Bruker Avance 500 (500.13 MHz). ¹H and ¹³C chemical shifts are reported in ppm with respect to tetramethylsilane and were measured using the resonances of the solvent (DMSO: ¹H δ 2.50 ppm, ¹³C δ 39.52 ppm) as internal standards, and the positions of the ¹²⁵Te resonances were referenced to an external standard solution of Ph₂Te₂ in CH₂Cl₂ (δ 420.36; ¹²⁵Te NMR) previously referenced to Me₂Te (δ 0.00; ¹²⁵Te NMR) as described elsewhere.² The diffuse-reflectance spectra were measured with an illuminated (tungsten halogen light source) integrating sphere (Ocean Optics ISP-REF) attached to a photodiode array spectrophotometer (Ocean Optics SD 2000) and are reported relative to a PTFE standard (Ocean Optics WS-1). Each measurement was an average of 100 scans that were integrated over 3 ms using a boxcar smoothing of 10 points and was corrected for stray light and dark current. High resolution electron-ionization mass spectrometry was performed on a Micro-mass GCT (GC-EI/CI time of flight) mass spectrometer. Melting points were measured on a Thomas-Hoover melting point apparatus and are reported uncorrected.

Second Harmonic Generation. A custom-built harmonic-light spectrometer⁷ was employed for these measurements. An Nd:YAG laser (Continuum Surelite II) was used as the light source. This system delivered IR pulses with a repetition frequency of 10 Hz, a width of 5–7 ns, and up to 655 mJ of energy at a wavelength of 1064 nm. A combination of an iris, a half-wave achromatic retarder, and a polarizer was used to modulate the intensity of the laser (*I_ω*), which was monitored with a photodiode with a 177 ps rise time (Newport Model 818-BB-30) and a beam splitter. The intensity of light scattered in the visible was measured with an end-on photomultiplier tube (Oriel 773346) with operating range 185–850 nm, gain above 5 × 10⁵, responsivity 3.4 × 10⁴ A/W, and rise time 15 ns. This detector received light through an assembly of an 850-nm cutoff short-pass filter (CVI); a crown-glass planoconvex lens of diameter 25.4 mm and focal length 50 mm; and an interferential filter (CVI) centered at 532 nm, with a nominal 10-nm fwhm spectral band. The PMT was normally operated under a 1000 V bias provided by a regulated power supply (Oriel 70705); the PMT output was delivered to a 350-MHz voltage amplifier (Oriel 70723). The responses of the two detectors were independently calibrated with a power meter (Melles Griot 13PEM001). The response of each detector was kept within its calibration range by means of neutral density filters (CVI) and measured with a boxcar integrator (Stanford Research 250), whose output was acquired with a digital oscilloscope card (National Instruments NI 5112 PCI) installed in a PC and controlled with a custom LabView Virtual Instrument.

The coefficient *d_{eff}* of each sample was evaluated by an adaptation of the Kurtz–Perry method⁷ using 7-mm-diameter pellets hand-pressed in a stainless steel die from freshly ground and sieved crystals. The averaged intensity of the signal (*I_{2ω}*) was fitted to

$$I_{2\omega} = Kd_{\text{eff}}^2 I_{\omega}^2 \quad (1)$$

where *I_ω* is the averaged intensity of the pump measured at the reference photodiode and *d_{eff}* = 1/2*χ*⁽²⁾. The calibration constant, *K*, was determined with a standard of KDP.

Synthesis of TeN₂C₂(CN)₂ (1b). TeCl₄ (0.10 g, 0.37 mmol) was dissolved in 3 mL of pyridine. This was added dropwise with stirring to a solution of diaminomaleonitrile (0.04 g, 0.37 mmol) in 3 mL of the same solvent. The mixture was stirred for an additional 5 min, and an excess of Et₃N (3.5 mmol, 0.5 mL) was added. Stirring was continued for 10 min, and the solution was filtered. A yellow solid was precipitated from the filtrate at –20 °C and filtered off. The final product was sublimed under dynamic vacuum (60 mTorr) at 100 °C to give a yellow powder. Yield after sublimation: 0.06 g (0.33 mmol, 89%), mp 130 °C (dec.). ¹³C{¹H} NMR (50 MHz, *d₆*-DMSO): δ 141.2 (4°); 119.3 (CN). ¹²⁵Te NMR (158 MHz, TeMe₂): δ 2408. Raman (cm⁻¹): 2224s, 1397vs, 1262w, 683vs, 538 m, 462w, 311s. IR (cm⁻¹): 2226 m, 1513vs, 1390 m, 1264vs, 1106vs, 705vs, 693vs, 576vs. EI HRMS *m/z* (ion, %, calc): 233.9181 (M⁺, 20, 231.9185), 181.9137 (M⁺ – 2CN, 20, 181.9124), 129.9027 (Te⁺, 100, 129.9062). Single crystals for X-ray diffraction were grown from pyridine at –20 °C.

The benzo-2,1,3-telluradiazoles, **3c** and **3d**, were prepared using a slightly different method in which TeCl₄ (0.16 g, 0.59 mmol) was dissolved in 3 mL of pyridine and added dropwise with stirring to a solution of 4,5-dichloro-*o*-phenylenediamine and 4-benzoyl-*o*-phenylenediamine, respectively (0.57 mmol), in 3 mL of the same solvent. The mixture was stirred for 5 min, and an excess of Et₃N (7 mmol, 1.0 mL) was added. Stirring was continued for 10 min, and toluene was added to the mixture to precipitate the product. The solid was washed three times with 5 mL of toluene. The crude product was recrystallized from pyridine and washed with 5 mL of toluene. The telluradiazole was separated from the Et₃N·HCl by density using CH₂Cl₂. The product obtained in this way could be further purified by an additional recrystallization and/or sublimation under vacuum as necessary. **TeN₂C₆H₂Cl₂ (3c):** Red/purple crystalline solid. Yield after recrystallization: 0.13 g (0.43 mmol, 76%), mp >200 °C. ¹H NMR (200 MHz, *d₆*-DMSO): δ 7.86 (s, 2H, aryl). Raman (cm⁻¹): 1487w, 1476w, 1415 m, 1349w, 1273s, 725w, 691s, 642w, 505w, 483w, 380w, 344m, 327w, 285w, 274m, 237s, 210w, 192m, 179s, 154m, 128m, 115vs. IR (cm⁻¹): 1487s, 1478m, 1417s, 1343m, 1270s, 1085vs, 979m, 852s, 84s, 825s, 727vs, 645w, 482m, 452vs. EI HRMS *m/z* (ion, %, calc): 301.8645 (M⁺, 20, 301.8657). Single crystals for X-ray diffraction were grown by slowly cooling down to room temperature a saturated solution prepared in pyridine at 100 °C. **TeN₂C₁₃H₈O (3d):** Orange crystalline solid. Yield after recrystallization: 0.23 g (0.48 mol, 86%), mp >200 °C. ¹H NMR (200 MHz, *d₆*-DMSO): δ 7.86, 7.82, 7.74, 7.72, 7.67, 7.63, 7.60, 7.56 (8H, m). ¹³C{¹H} NMR (50 MHz, *d₆*-DMSO): δ 132.5 (1C, 3°), 131.1 (1C, 3°), 129.3 (2C, 3°), 128.4 (2C, 3°), 128.1 (1C, 3°), 125.6 (1C, 3°). Raman (cm⁻¹): 1641s, 1597m, 1488w, 1427s, 1347w, 1326m, 1298s, 1139w, 1115w, 1025w, 996w, 788vw, 754vw, 689vs, 562w, 399m, 338w, 305w, 274w, 214vs, 165m. IR (cm⁻¹): 3056w, 1642vs, 1595m, 1577w, 1516w, 1493w, 1446m, 1433w, 1329s, 1310m, 1301m, 1238s, 1175w, 1141w, 1117w, 960w, 940w, 890s, 883m, 822m, 805m, 791m, 718vs, 705m, 682m, 630w, 594w, 565w, 509w, 439m. EI HRMS *m/z* (ion, %, calc): 337.9678 (M⁺, 50, 337.9699). Single crystals for X-ray diffraction were grown by sublimation under static vacuum at 120 °C.

X-ray Crystallography. All samples were handled under Paratone-N oil (Hampton Research) at room temperature. Crystals of **1b** (0.42 × 0.40 × 0.07 mm³), **3c** (0.60 × 0.10 × 0.08 mm³), and **3d** (0.40 × 0.20 × 0.01 mm³) were mounted on MiTeGen Micromounts (Ithaca, NY) using Paratone-N oil. Data for **1b** and **3d** were collected on a SMART APEX II diffractometer utilizing Mo Kα radiation (λ = 0.71073 Å, graphite monochromator) and equipped with an Oxford cryostream 700 low temperature accessory. Data for **3c** were collected on a P4 Bruker diffractometer upgraded with a Bruker SMART 1K CCD detector and a rotating anode utilizing Mo Kα radiation (λ = 0.71073 Å, graphite monochromator) and equipped with an Oxford Cryostream 700 low temperature accessory. Redundant data sets were collected, in 0.36° steps in φ or ω, with a crystal-to-detector distance of 4.947 cm for **1b**, 4.999 cm for **3c**, and 4.958 cm for **3d**. Preliminary orientation matrices were obtained from the first frames using the Bruker APEX2 software suite⁸ for **1b** and **3c** and CELL_NOW⁹ for **3d**. The final cell

Table 1. Crystallographic and Refinement Parameters for **1b**, **3c**, and **3d**

compound	1b	3c	3d
empirical formula	C ₄ N ₄ Te	C ₆ H ₂ Cl ₂ N ₂ Te	C ₁₃ H ₈ N ₂ O ₂ Te
crystal system	orthorhombic	orthorhombic	monoclinic
space group	<i>P</i> 2 ₁ 2 ₁ 2 ₁	<i>Pca</i> 2 ₁	<i>C</i> 2
<i>a</i> (Å)	5.983(2)	7.588(2)	10.647(7)
<i>b</i> (Å)	7.781(3)	7.744(2)	7.761(5)
<i>c</i> (Å)	12.932(5)	28.008(6)	14.31(1)
α (deg)	90	90	90
β (deg)	90	90	96.78(2)
γ (deg)	90	90	90
<i>V</i> (Å ³)	602.0(4)	1645.9(6)	1174(1)
<i>Z</i> , ρ(calc) (g·cm ⁻³)	4, 2.556	8, 2.426	4, 1.900
<i>T</i> (K)	173(2)	173(2)	173(2)
μ (mm ⁻¹)	4.840	4.192	2.516
θ range	3.06–32.03	1.45–28.85	2.87–23.28
limiting indices	−8 ≤ <i>h</i> ≤ 8 −11 ≤ <i>k</i> ≤ 8 −19 ≤ <i>l</i> ≤ 18	−8 ≤ <i>h</i> ≤ 9 −10 ≤ <i>k</i> ≤ 10 −37 ≤ <i>l</i> ≤ 37	−10 ≤ <i>h</i> ≤ 11 0 ≤ <i>k</i> ≤ 8 0 ≤ <i>l</i> ≤ 15
refl collec/unique	9691/2087	12915/3931	1164/1164
<i>R</i> (int)	0.0748	0.0870	0.0000
no. of parameters	83	200	155
twin fraction	0.244	0.360	0.440
twinning	racemic	racemic	180°; [001]
<i>R</i> ¹ / <i>wR</i> ² (<i>I</i> > 2σ(<i>I</i>))	0.0451/0.0835	0.0634/0.1561	0.0546/0.1100
<i>R</i> ¹ / <i>wR</i> ² for all data	0.0696/0.0909	0.1085/0.1732	0.0722/0.1157
goodness-of-fit on <i>F</i> ²	0.987	1.058	1.021
larg diff peak/hole (e [−] Å ^{−3})	2.302/−1.097	2.738/−2.178	1.508/−1.212

$$^a R1 = \sum ||F_o| - |F_c|| / \sum |F_o|; wR2 = \{ \sum [w(F_o^2 - F_c^2)^2] / \sum w(F_o^2) \}^{1/2}$$

parameters were obtained by refinement on the positions of selected reflections with $I > 10\sigma(I)$ after integration of all the frames using the Bruker APEX2 software suite⁸ for each of **1b**, **3c**, and **3d**. The data was empirically corrected for absorption and other effects using the Bruker APEX2 software suite;⁸ **3d** data was corrected using TWINABS.¹⁰ The structures were solved by Patterson heavy atom methods and refined by full-matrix least-squares on all F2 data using SHELXL¹¹ as part of the WinGX package.¹² The non-H atoms were refined anisotropically, while H atoms were constrained to idealized positions using appropriate riding models. Molecular graphics were produced using ORTEP-3¹³ or Mercury 2.2.¹⁴

Computational Methods. The structures considered in this study were fully optimized using the ADF DFT package (SCM, versions 2008.01 to 2009.01).^{15–17} The Adiabatic Local Density Approximation (ALDA) was used for the exchange-correlation kernel,^{18,19} and the differentiated static LDA expression was used with the Vosko-Wilk-Nusair parametrization.²⁰ The calculations of model geometries were gradient-corrected with the exchange and correlation functionals of the gradient correction proposed by Perdew and Wang,^{21,22} which usually reproduces satisfactorily the geometries of heavy main-group systems.²³ Geometry optimizations were conducted using a triple- ζ all-electron basis set with one polarization function and applying the zeroth order regular approximation (ZORA) with specially adapted basis sets.^{24–28} Geometry constraints were used when point group symmetry was applicable. Visualization of the computational results was performed using the ADF-GUI.²⁹

Results and Discussion

Design Rationale. Interest in materials with crystal structures that lack an inversion center derives, in great part, from their potential applications in optical technologies.^{30,31} It can be shown that because their even-order dielectric susceptibilities ($\chi^{(n)}$) are different from zero, their macroscopic polarization (P , eq 2) enables interactions with electric fields (E)—including those of optical origin—that result in phenomena such as the electro-optic Pockels effect and Second Harmonic Generation (SHG).

$$P = \chi^{(1)}E + \chi^{(2)}EE + \chi^{(3)}EEE + \dots \quad (2)$$

Table 2. Selected Bond Distances and Angles for **1b**, **3c**, and **3d**

	1b	3c^a	3d
Intramolecular			
Te–N1 (Å)*	2.022(6)	2.01(1), 2.04(2)	2.02(1)
Te–N2 (Å)*	2.035(6)	2.02(1), 2.05(2)	2.03(2)
N1=C (Å)*	1.300(9)	1.33(2), 1.29(2)	1.29(2)
N2=C (Å)*	1.306(9)	1.36(2), 1.28(2)	1.29(2)
C–C (Å)*	1.443(8)	1.45(2), 1.46(2)	1.50(2)
N–Te–N (deg)*	82.5(2)	84.2(6), 84.4(6)	82.8(5)
Te–N1=C (deg)*	111.1(5)	112(1), 108(1)	112(1)
Te–N2=C (deg)*	109.9(4)	109(1), 108(1)	111(1)
Intermolecular			
Te···N1 (Å)*	2.767(6)	2.51(1), 2.54(1)	2.68(2)
Te···N2 (Å)*	2.659(6)	2.89(1), 2.87(1)	2.80(2)
N2–Te···N1 (deg)*	67.1(2)	72.4(5), 73.2(5)	71.6(6)
N1–Te···N2 (deg)*	69.6(2)	64.2(5), 65.8(5)	68.8(5)
Te–N1–Te (deg)*	109.7(2)	104.9(6), 103.3(6)	107.7(7)
Te–N2–Te (deg)*	113.5(2)	118.2(7), 117.5(6)	111.8(7)

^aThe measurements are duplicated because the asymmetric unit consists of two molecules; the two sets are equal within 3σ.

While a number of inorganic crystals, such as β -BaB₂O₄, are now routinely used in tunable coherent light sources, the rational design of nonlinear optical (NLO) supramolecular materials remains an important topic of research. The most straightforward approach in this area relies on using strong, well-defined supramolecular interactions to influence the organization of molecules in the lattice. In this context, hydrogen bonding has been used to engineer acentric crystal lattices.^{32,33} For example, benzoic acids that form acentric ribbon chains tend to crystallize in acentric space groups, as is observed in 11 of 21 cited examples.³⁴ Of these, the ortho-substituted rings show the highest preference for acentric spatial arrangement as a result of interchain interactions. The use of noncentrosymmetric supramolecular ribbons to promote a noncentric lattice has been extended to include other types of supramolecular interactions. There are several examples of coordination polymers with acentric bridging ligands that promote acentric lattice formation.^{35–37} It is, therefore, reasonable to expect that noncentrosymmetric distortions to the [Te–N]₂ synthon could be used to build noncentrosymmetric ribbon chains and noncentrosymmetric crystals. This approach requires the identification of molecular building blocks for which the steric repulsion would be sufficient to cause the distortion but not so large as to prevent association. With this in mind, we chose to investigate the structures of 3,4-dicyano-1,2,5-telluradiazole (**1b**) and 5,6-dichlorobenzo-2,1,3-telluradiazole (**3c**), which can be conveniently prepared with small modifications of the published general method² from readily available diamines.

Crystal Structures of **1b and **3c**.** Crystallographic data and final refinement parameters for all new compounds are collected in Table 1, and selected bond distances and angles are presented in Table 2. The crystal structures of **1b** and **3c** display the expected ribbon chains and do crystallize in noncentrosymmetric space groups (Figures 1–4). There are one and two molecules in the asymmetric units of **1b** and **3c**, respectively. Considering the magnitudes of the standard deviations in bond lengths and angles, both molecules have a pseudo-C_{2v} symmetry. Both systems are essentially planar, within the magnitudes of the standard deviations. Also, there are no significant differences between the molecular dimensions of **1b** and **1a** or between those of **3c** and **3b**. In both instances, the ribbon chains are assembled along the [0, 1, 0] axis by the [Te–N]₂ supramolecular synthon but with

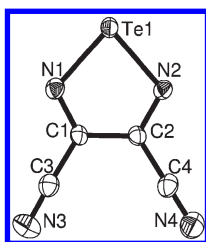


Figure 1. ORTEP and numbering scheme for the asymmetric unit in the crystal structure of **1b**. Displacement ellipsoids are shown at the 50% probability level.

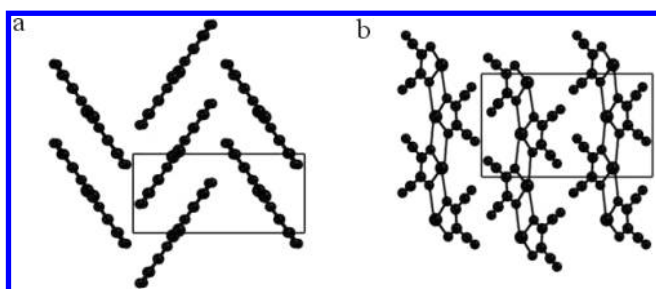


Figure 2. Ball and stick representation of two views of the crystal structure of **1b**: (a) along (0, 1, 0) and (b) along (1, 0, 0).

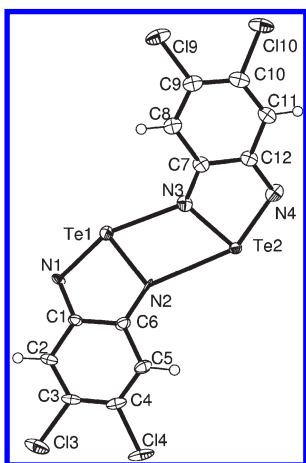


Figure 3. ORTEP and numbering scheme for the asymmetric unit in the crystal structure of **3c**. Displacement ellipsoids are shown at the 50% probability level.

significant distortions. The associated heterocycles are not coplanar, having a $4.7(1)^\circ$ rotation between adjacent heterocycles in the crystal of **1b** and $5.5(3)^\circ$ in **3c**. This deviation is smaller than the $12.0(4)$ and $10.8(5)^\circ$ observed in α -**3a** but larger than the $2.5(4)^\circ$ in the case of **1a**. The noncentrosymmetric distortion of the $[\text{Te}-\text{N}]_2$ supramolecular synthon is also apparent in the asymmetry of $\text{Te}\cdots\text{N}$ SBIs; these differ by 0.108 \AA in **1b** and an average of 0.36 \AA in **3c**. In the latter case, this difference is even larger than the 0.26 \AA observed in α -**3a**.

NLO Properties of 1b and 3c. The SHG efficiency of crystalline samples of **1b** and **3c** was examined by evaluating the d_{eff} coefficient using the Kurtz–Perry method with a fundamental wavelength of 1064 nm (Figure 5). Although twinning has a detrimental effect on the NLO activity of single crystals, its impact is less significant in the collective response of randomly oriented microcrystals.^{38–40} The values determined for **1b** and **3c** were respectively 0.136 ± 0.001 and 0.089 ± 0.002 times the magnitude of the standard

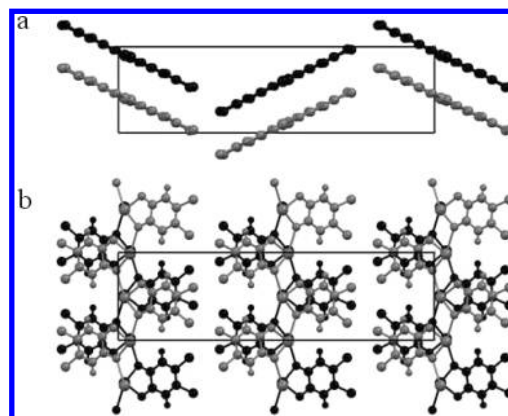


Figure 4. Two views of the crystal structure of **3c**: (a) along (0, 1, 0); (b) along (1, 0, 0). Models presented as ball and stick; different layers are represented with different shades of gray for clarity.

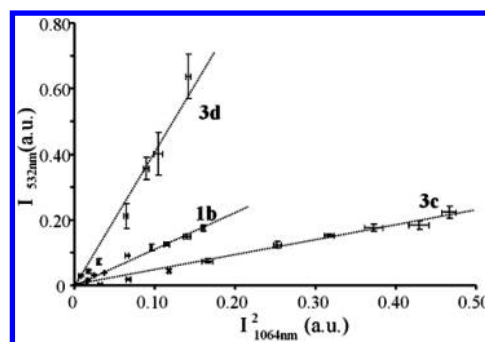


Figure 5. Kurtz–Perry SHG measurements for **1b**, **3c**, and **3d**.

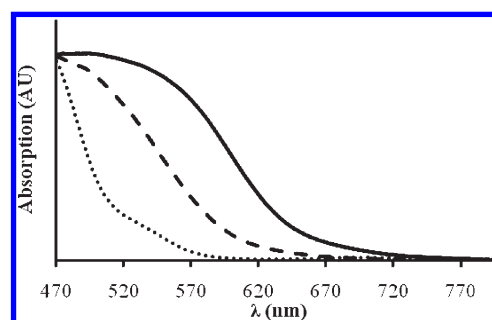


Figure 6. Diffuse reflectance spectra in the visible of **1b** (\cdots), **3c** ($—$), and **3d** ($---$).

of KH_2PO_4 (KDP, $d_{\text{eff}} = 0.39 \text{ pm/V}$).⁴¹ These values are small and might be subject to the competing effects of resonant enhancement and absorption at the wavelength of the second harmonic (520 nm), as the diffuse reflectance spectra of these samples suggest (Figure 6). Despite the small magnitude of d_{eff} , these results do confirm that the crystals of **1b** and **3c** possess a second-order NLO response as a result of their noncentrosymmetric lattice. The limited solubility of the compounds precluded accurate measurements of their hyperpolarizabilities in solution; thus, their hyperpolarizability tensors were calculated using TD-DFT. To aid in the interpretation, the calculations were expanded to include **1a**, **3b**, and *p*-nitroaniline (**4**). For these calculations, single molecule models were fully optimized, with appropriate symmetry constraints. The results are presented in Table 3. For convenience and because it is the quantity measurable by hyper-Rayleigh scattering, only the orientational average of each tensor ($\langle\beta\rangle$) is used. The HOMO–LUMO gaps and dipole

Table 3. DFT and TD-DFT Calculated Values Relevant to the NLO Activity

compound	1b	1a	3d	3c	3b	4
static $\langle\beta\rangle$ (esu $\times 10^{30}$)	2.79	1.60	1.94	8.08	1.93	8.44
SHG ₁₀₆₄ $\langle\beta\rangle$ (esu $\times 10^{30}$)	3.55	1.68	2.99	15.58	1.88	18.62
μ (D)	6.99	0.04	3.22	2.32	0.13	7.91
HOMO–LUMO gap (eV)	2.84	3.14	2.23	2.33	2.45	2.67

moments are also included in Table 3. Translating the calculated tensors to the macroscopic susceptibilities would require intermolecular interactions in addition to the geometric and local field effects to be accounted for,^{42–44} which are outside the scope of this work. Nevertheless, the calculated data is very informative. The calculations do show that the 1,2,5-telluradiazole and the small modifications here considered are chromophores with reasonable hyperpolarizabilities, comparable to that of **4** in the best case. The orientation of the molecules is one of the factors that give the observed small SHG efficiencies. The point group of **1b**, $P2_12_12_1$, is nonpolar, and thus, there is a mutual cancellation of the molecular dipole moments causing the macroscopic nonlinear response to arise only from the octopolar terms of the second-order susceptibility tensor. On the other hand, the point group of **3c** is polar with an overall dipole parallel to the [0, 0, 1] axis. The molecular dipoles, however, are aligned in a nearly antiparallel fashion. DFT calculations on the asymmetric unit (the SBI dimer) of **3c** gave an overall dipole moment of 1.95 D, but its projection along the [0, 0, 1] axis is only 0.25 D.

Extension to a Monosubstituted Benzo-2,1,3-telluradiazole.

As the example of **3c** illustrates, formation of ribbon chains necessarily places the molecular dipoles in a nearly antiparallel orientation which will cancel most of the NLO activity. Therefore, in order to design and build a more efficient NLO material, the distortion of the [Te–N]₂ supramolecular synthon could only be used as a means to induce noncentrosymmetric packing. It would be indispensable, then, to append chromophores with larger hyperpolarizabilities and promote an alignment that preserves molecular dipoles. Simultaneously, the steric bulk of chromophore groups should distort the [Te–N]₂ supramolecular synthon yet not prevent the formation of the ribbons. One way in which all of this could be accomplished is by attaching the chromophore at the 3- or 5-positions of **1** or **2**, respectively. To explore this concept, the commercially available 3,4-diaminobenzophenone was used to prepare **3d**. X-ray crystallography revealed a unit cell with an asymmetric unit consisting of one molecule (Figure 7). The internal parameters of the five-membered heterocycle are the same as in the previously discussed structures, within the standard deviations. As in the previous examples, supramolecular ribbon chains are assembled by a distorted [Te–N]₂ supramolecular synthon along a screw axis perpendicular to the *ac* plane (Figure 8). The angle of rotation between neighboring telluradiazole rings is 1.2(4)°, and the difference in Te···N SBI distances is 0.12 Å. The benzoyl group is rotated by 51(1)° from the plane of the benzo-2,1,3-telluradiazole and is interdigitated with the corresponding groups pendant from the neighboring ribbons. This π -stacking interaction appears to facilitate the propagation of noncentrosymmetry throughout the lattice. The magnitude of d_{eff} for **3d** was found to be 0.261 ± 0.003 times that of KDP. The average of the molecular hyperpolarizability calculated by TD-DFT (Table 3) is comparable to the other values. The diffuse reflectance spectrum of this compound is also shown in Figure 6 and shows significant

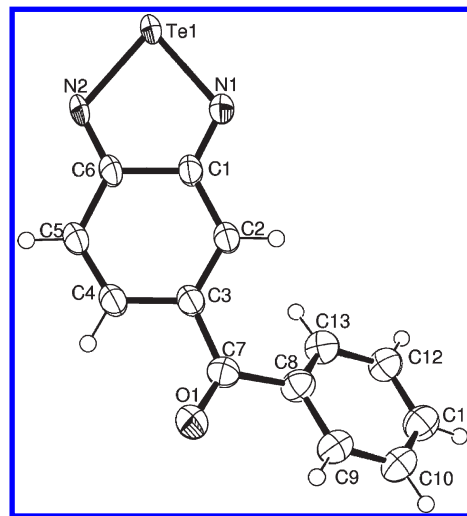


Figure 7. ORTEP and numbering scheme for the asymmetric unit in the crystal structure of **3d**. Displacement ellipsoids are shown at the 50% probability level.

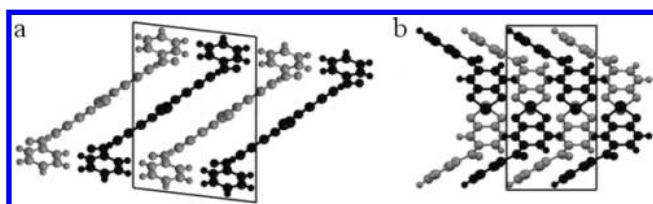


Figure 8. Two views of the crystal structure of **3d**: (a) along (0, 1, 0); and (b) along (1, 0, 0). The ball and stick models portray different layers in distinct shades of gray for clarity.

absorption at 520 nm. In this case, the point group of the lattice is polar with an overall dipole parallel to the [0, 1, 0] axis; the projection of each molecular dipole moment along this direction is 1.94 D.

Concluding Remarks. It has been previously shown in several instances that supramolecular interactions such as hydrogen bonding can promote noncentrosymmetric packing and thus drive the assembly of NLO crystals.^{32,33} There are, however, situations in which the use of other intermolecular forces would be advantageous. For example, in a hydrogen-bonded NLO material intended for use in electro-optic modulators, absorption by the vibrational overtones of N–H and O–H bonds would have a detrimental effect at the near-infrared wavelengths used in current silica optical fiber technology.^{45,46} Supramolecular interactions between heavy elements, e.g. main-group SBIs, would give materials with greater near-infrared transparency because their overtones appear at much longer wavelengths.

Earlier work showed that the interaction between iodo and nitro functional groups, on its own⁴⁷ and in combination with hydrogen bonds,⁴⁸ can promote parallel alignment of NLO chromophores in crystal structures. The approach demonstrated in this report relies on the distortion of a supramolecular synthon to create a noncentrosymmetric feature that is able to propagate through the lattice and can, in principle, be extended to create NLO crystals of functionalized benzo-2,1,3-telluradiazoles.

Acknowledgment. We acknowledge the continuous support of NSERC Canada (IVB Discovery Grant, AFC Scholarship), the Canada Foundation for Innovation, and

the Ontario Innovation Fund. This work was made possible by the facilities of the Shared Hierarchical Academic Research Computing Network (SHARCNET: www.sharcnet.ca) and Compute/Calcul Canada.

Supporting Information Available: Crystallographic information files (CIF) for **1b**, **3d**, and **3d**. This material is available free of charge via the Internet at <http://pubs.acs.org>.

References

- Bertini, V.; Dapporto, P.; Lucchesini, F.; Segal, A.; Munno, A. D. *Acta Crystallogr., C* **1984**, *40*, 653.
- Cozzolino, A. F.; Britten, J. F.; Vargas-Baca, I. *Cryst. Growth Des.* **2006**, *6*, 181–186.
- Neidlein, R.; Knecht, D.; Gieren, A.; Ruiz-Perez, C. Z. *Naturforsch. B* **1987**, *42*, 84.
- Chivers, T.; Gao, X.; Parvez, M. *Inorg. Chem.* **1996**, *35*, 9.
- Desiraju, G. R. *Angew. Chem., Int. Ed. Engl.* **1995**, *34*, 2311–2327.
- Cozzolino, A. F.; Whitfield, P.; Vargas-Baca, I. *J. Am. Chem. Soc.*, in press.
- Zhang, W.; Cozzolino, A. F.; Mahmoudkhani, A. H.; Tulumello, M.; Mansour, S.; Vargas-Baca, I. *J. Phys. Chem. B* **2005**, *109*, 18378–18384.
- Bruker **2006**; APEX2. Bruker AXS Inc.: Madison, WI.
- Sheldrick, G. M. *CELL_NOW*; University of Göttingen: Göttingen, **2003**.
- Sheldrick, G. M. *TWINABS*, **2002**; University of Göttingen: Germany, **2002**.
- Sheldrick, G. M. *SHELX97 [Includes SHELXS97, SHELXL97, CIFTAB]—Programs for Crystal Structure Analysis (Release 97-2)*; Institut für Anorganische Chemie der Universität: Tammanstrasse 4, D-3400 Göttingen, Germany, **1998**.
- Farrugia, L. J. *J. Appl. Crystallogr.* **1999**, *32*, 837–838.
- Farrugia, L. J. *J. Appl. Crystallogr.* **1997**, *30*, 565.
- Macrae, C. F.; Edgington, P. R.; McCabe, P.; Pidcock, E.; Shields, G. P.; Taylor, R.; Towler, M.; van de Streek, J. *J. Appl. Crystallogr.* **2006**, *39*, 453–457.
- Te Velde, G.; Bickelhaupt, F. M.; Baerends, E. J.; Fonseca Guerra, C.; Van Gisbergen, S. J. A.; Snijders, J. G.; Ziegler, T. *J. Comput. Chem.* **2001**, *22*, 931–967.
- Guerra, C. F.; Snijders, J. G.; Velde, G. t.; Baerends, E. J. *Theor. Chem. Acc.* **1998**, *99*, 391.
- Baerends, E. J.; Autschbach, J.; Bashford, D.; Bérces, A.; Bickelhaupt, F. M.; Bo, C.; Boerrigter, P. M.; Cavallo, L.; Chong, D. P.; Deng, L.; Dickson, R. M.; Ellis, D. E.; Faassen, M. v.; Fan, L.; Fischer, T. H.; Guerra, C. F.; Ghysels, A.; Giammona, A.; Gisbergen, S. J. A. v.; Götz, A. W.; Groeneveld, J. A.; Gritsenko, O. V.; Grüning, M.; Harris, F. E.; Hoek, P. v. d.; Jacob, C. R.; Jacobsen, H.; Jensen, L.; Kessel, G. v.; Kootstra, F.; Krykunov, M. V.; Lenthe, E. v.; McCormack, D. A.; Michalak, A.; Mitoraj, M.; Neugebauer, J.; Nicu, V. P.; Noodleman, L.; Osinga, V. P.; Patchkovskii, S.; Philipsen, P. H. T.; Post, D.; Pye, C. C.; Ravenek, W.; Rodríguez, J. I.; Ros, P.; Schipper, P. R. T.; Schreckenbach, H. G.; Seth, M.; Snijders, J. G.; Solà, M.; Swart, M.; Swerhone, D.; Velde, G. t.; Vernooijs, P.; Versluis, L.; Visser, O.; Wang, F.; Wesolowski, T. A.; Wezenbeek, E. v.; Wiesenecker, G.; Wolff, S. K.; Woo, T. K.; Yakovlev, A. L.; Ziegler, T. *ADF* 2009.01; SCM, Theoretical Chemistry, Vrije Universiteit: Amsterdam, The Netherlands, <http://www.scm.com>.
- van Gisbergen, S. J. A.; Snijders, J. G.; Baerends, E. J. *Phys. Rev. Lett.* **1997**, *78*, 3097–3100.
- van Gisbergen, S. J. A.; Snijders, J. G.; Baerends, E. J. *J. Chem. Phys.* **1998**, *109*, 10644–10656.
- Vosko, S. H.; Wilk, L.; Nusair, M. *Can. J. Phys.* **1980**, *58*, 1200–11.
- Perdew, J. P. *Phys. Rev. B* **1986**, *33*, 8822.
- Perdew, J. P.; Wang, Y. *Phys. Rev. B* **1992**, *45*, 13244.
- Leigh, W. J.; Harrington, C. R.; Vargas-Baca, I. *J. Am. Chem. Soc.* **2004**, *126*, 16105–16116.
- van Lenthe, E.; Ehlers, A.; Baerends, E.-J. *J. Chem. Phys.* **1999**, *110*, 8943–8953.
- van Lenthe, E.; Baerends, E. J.; Snijders, J. G. *J. Chem. Phys.* **1993**, *99*, 4597–610.
- van Lenthe, E.; Baerends, E. J.; Snijders, J. G. *J. Chem. Phys.* **1994**, *101*, 9783–92.
- van Lenthe, E.; Snijders, J. G.; Baerends, E. J. *J. Chem. Phys.* **1996**, *105*, 6505–6516.
- van Lenthe, E.; van Leeuwen, R.; Baerends, E. J.; Snijders, J. G. *Int. J. Quantum Chem.* **1996**, *57*, 281–93.
- ADF-GUI*, 2009.01; SCM: Amsterdam, The Netherlands, <http://www.scm.com>.
- Kellner, T.; Heine, F.; Huber, G. *Appl. Phys. B: Lasers Opt.* **1997**, *65*, 789–792.
- Lee, M.; Katz, H. E.; Erben, C.; Gill, D. M.; Gopalan, P.; Heber, J. D.; McGee, D. J. *Science* **2002**, *298*, 1401–1403.
- Etter, M. C.; Frankenbach, G. M.; Adsmund, D. A. *Mol. Cryst. Liq. Cryst.* **1990**, *187*, 25–25.
- Kadirvelraj, R.; Umarji, A. M.; Robinson, W. T.; Bhattacharya, S.; Guru Row, T. N. *Chem. Mater.* **1996**, *8*, 2313–2323.
- Frankenbach, G. M.; Etter, M. C. *Chem. Mater.* **1992**, *4*, 272–278.
- Hao, Z.-M.; Zhang, X.-M. *Cryst. Growth Des.* **2008**, *8*, 2359–2363.
- Qu, Z.-R.; Hong, Z.; Yi-Ping, W.; Xi-Sen, W.; Qiong, Y.; Yong-Hua, L.; Ren-Gen, X.; Brendan, F. A.; Zhi-Guo, L.; Zi-Ling, X.; Xiao-Zeng, Y. *Chem.—Eur. J.* **2004**, *10*, 53–60.
- Huang, X.-F.; Li, Y.-H.; Wu, Q.; Ye, Q.; Xiong, R.-G. *Inorg. Chim. Acta* **2005**, *358*, 2097–2100.
- Hagemann, M.; Weber, H. J. *J. Appl. Phys. A: Mater. Sci. Process.* **1996**, *63*, 67–74.
- Bourgogne, C.; Fur, Y. L.; Juen, P.; Masson, P.; Nicoud, J.-F.; Masse, R. *Chem. Mater.* **2000**, *12*, 1025–1033.
- Rechsteiner, P.; Hulliger, J.; Florsheimer, M. *Chem. Mater.* **2000**, *12*, 3296–3300.
- Craxton, R.; Jacobs, S.; Rizzo, J.; Boni, R. *IEEE J. Quantum Electron.* **1981**, *17*, 1782–1786.
- Zyss, J.; Oudar, J. L. *Phys. Rev. A* **1982**, *26*, 2028.
- Zyss, J.; Berthier, G. *J. Chem. Phys.* **1982**, *77*, 3635–3654.
- Dirk, C. W.; Twieg, R. J.; Wagniere, G. *J. Am. Chem. Soc.* **1986**, *108*, 5387–5395.
- Takezawa, Y.; Noriaki, T.; Seikichi, T.; Shuichi, O. *J. Polym. Sci., Part B: Polym. Phys.* **1992**, *30*, 879–885.
- Thomas, G. A.; Shraiman, B. I.; Glodis, P. F.; Stephen, M. J. *Nature* **2000**, *404*, 262–264.
- Sarma, J. A. R. P.; Allen, F. H.; Hoy, V. J.; Howard, J. A. K.; Thaimattam, R.; Biradha, K.; Desiraju, G. R. *Chem. Commun.* **1997**, 101–102.
- George, S.; Nangia, A.; Lam, C.-K.; Mak, T. C. W.; Nicoud, J.-F. *Chem. Commun.* **2004**, 1202–1203.